Desalination and Water Treatment
www.deswater.com
doi: 10.1080/19443994.2015.1040467

57 (2016) 10546–10559
May

Taylor & Francis
Taylor & Francis Group

Numerical simulation of the electrodeionization (EDI) process with layered resin bed for deeply separating salt ions

Jun Lu[a,*], Xiao-Yun Ma[a], Yu-Xin Wang[b]

[a]*School of Environmental and Chemical Engineering, Jiangsu University of Science and Technology, Zhenjiang, Jiangsu 212003, China, Tel. +86 511 84401181; emails: jluabc@163.com (J. Lu), maxiaoyun1836289@163.com (X.-Y. Ma)*
[b]*School of Chemical Engineering and Technology, Tianjin University, Tianjin 300072, China, Tel. +86 22 27890515; email: yxwang@tju.edu.cn*

Received 23 October 2014; Accepted 4 April 2015

ABSTRACT

A numerical steady state model was established to describe electrodeionization (EDI) process, the dilute compartment (DC) of which is fixed with layered resin bed (LayeredEDI). The water dissociation influence on current efficiency was considered. The risk of hydroxide precipitation in dilute and concentrated compartment (CC) was investigated. It was found that in LayeredEDI the risk of hydroxide precipitation at anion-exchange membrane (AM) surface is reduced. However, there exist two OH^- concentration peaks at AM surface in CC. The hydroxide precipitation usually exists on these areas. The simulation results show that in DC, the hydroxide precipitation is negligible. The highest concentration area is near cation-exchange membrane–cation resin bed interface.

Keywords: Electrodeionization; Electrodialysis; Water dissociation; Ion-exchange; Membrane

1. Introduction

The electrodeionization (EDI) process, which combines ion-exchange and electrodialysis, is a green and environment-friendly process for deeply separating salt ions [1]. The EDI process is now commonly used for producing ultrapure water and deeply separating heavy metal ions [2–6]. EDI process for treating low-concentration solutions has some advantages. Compared with the ion-exchange process, the EDI *in situ* regenerates the ion-exchange resins (no acid and alkali is used). Compared with the electrodialysis, EDI process with ion-exchange resins fixed in dilute compartment (DC) has ionic channels with high conductivity for salt ion transfer. EDI process has the advantage of lower energy consumption and no additional chemicals. Further more, nowadays the demand for deeply separating heavy metal ions in nuclear power plant and electroplating industry is urgent. With those advantages, EDI technology for deeply separating solutions with low-level heavy metal ions is receiving great attentions [7–15].

The EDI with DC fixed with cation-exchange resin (CREDI) is used to deeply separate heavy metal ions. In CREDI, the intense water dissociation at DC anion-exchange membrane (AM) interface causes a low current efficiency. The water dissociation product OH^- combines with heavy metal ions at the interface of cation-exchange membrane (CM) and concentrated compartment (CC) to form precipitations in CC (Fig. 1). The low current efficiency and hydroxide precipitation

*Corresponding author.

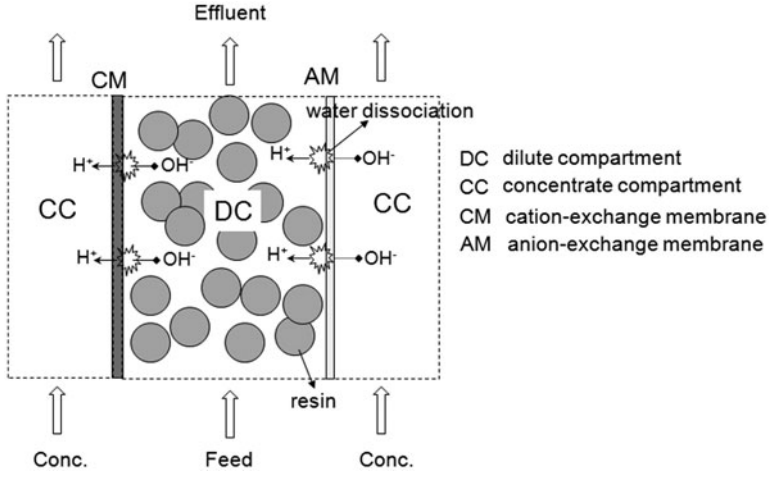

Fig. 1. Illustration of water dissociation and ionic transportation in EDI [12].

at membrane surface make the CREDI not suitable for separating heavy metal ions [7,9,10,13].

The water dissociation products, which can carry currents, will lead to the decrease of current efficiency. In addition, the water dissociation product OH^- can lead to the risk of precipitation of metal hydroxides. However, water dissociation in EDI is useful and necessary for deeply separating salt ions [7,12,15,16]. Thus, the optimal state is that the salt ions are deeply removed and only necessary water dissociation takes place [12,16].

In our previous study [12,16], it was found that at the same target removal percentage, the current efficiency of EDI with DC fixed with mixed cation and anion-exchange resins (MixREDI) is much larger than that of CREDI (i.e. the excessive water dissociation produced in MixREDI is lower than that of CREDI). However, if the MixREDI is used to remove the heavy metal ions, metal hydroxide precipitation will exist in DC (the concentration of OH^- near the CM in DC is much large [12]). (In general, if EDI is used to treating heavy metal ions, it has the risk of precipitation. So far, it is hard to identify or measure the place where the precipitation will take place. Thus, the area where the concentration of OH^- is much high will be the place where precipitation reaction may take place.) This is the reason why the MixREDI is not suitable for separating heavy metal ions.

The most intense concentration polarization exists at the outlet area [12,16]. At the outlet area, water dissociation current increases dramatically at the streamline direction. Thus, the local current efficiency decreases dramatically at the outlet area [16]. Therefore, the current efficiency of the whole cell almost depends on the water dissociation intensity at the outlet area. It is also necessary to mention that the intense water dissociation at outlet area could bring with serious precipitations at AM–CC interface. Water dissociation depends on the concentration polarization condition, which is controlled by stack configuration of resin bed. Thus, the stack configuration should be adjusted to make appropriate water dissociation.

Generally, the DC of EDI is filled with CREDIs [8,14,17]. In our previous work [12,16], it was found that the EDI with this stack configuration produces excessive water dissociation products. A layered stack configuration of resin bed was developed by Yeon et al. [7]. This stack configuration was reported to substantially reduce the risk of hydroxide precipitation. EDI with this stack configuration is named LayeredEDI. However, limited by the measuring technique, the quantification of water dissociation in the EDI with this configuration was seldom investigated. The water dissociation intensity should be measured to quantify the hydroxide precipitation condition in DC and CC.

The purpose of this study was to simulate the LayeredEDI process for deeply separating salt ions. A 2D model was established. The concentration distribution of water dissociation products in dilute and CC is obtained. The positions where the hydroxide precipitation may occur are recognized.

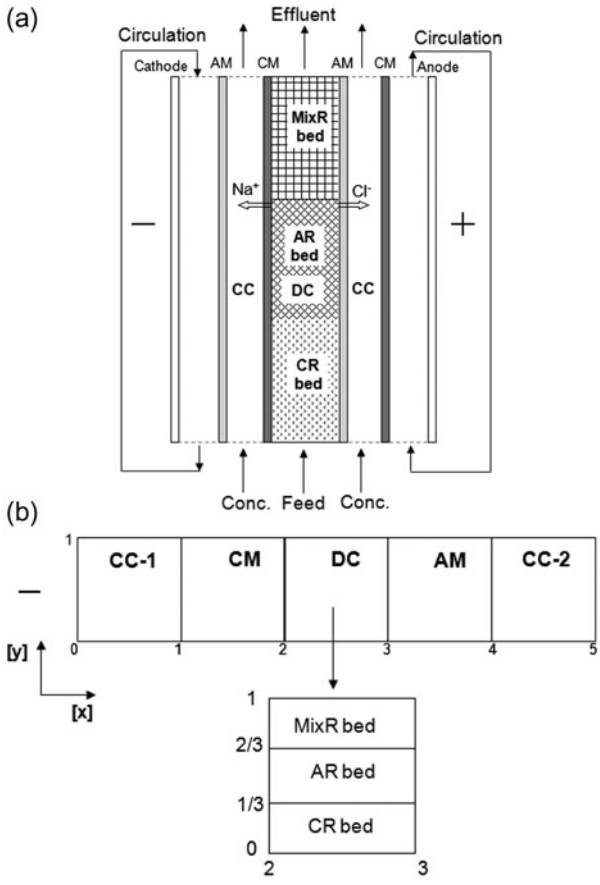

Fig. 2. The real (a) and dimensionless domain (b) of EDI cell for the numerical simulation. CC-1: left CC. CM: cation membrane. DC: dilute compartment. AM: anion membrane. CC-2: right CC. MixR bed: mixed cation-exchange and anion-exchange resin bed. AR bed: anion-exchange resin bed. CR bed: cation-exchange resin bed [12,16].

2. Mathematical formulation

2.1. Problem statement

The real and dimensionless domain of EDI cell for the numerical simulation was illustrated in Fig. 2 [12,16]. The DC is filled with three layers. From the inlet to the outlet, they are cation resin bed (CR bed), anion resin bed (AR bed), and mixed resin bed (MixR bed). Parameters of the model were shown in Table 1. The NaCl solution is considered as the influent of CC and DC. The ionic species in our model are Na^+, Cl^-, H^+, and OH^- and denoted as species 1, 2, 3, and 4, respectively.

The thickness of dilute and CC (DC and CC) is both set as 4 mm. NaCl concentration of DC's feed water is 0.1 mol m^{-3}. Influent velocity of CC is 0.05 m s^{-1}. NaCl concentration of CC's feed water is 1 mol m^{-3}. Influent velocity of CC is 0.05 m s^{-1}. The thickness of cation-exchange and AM (CM and AM) is both set as 0.4 mm. Ion-exchange capacity of CM and AM is both set as 1,000 mol m^{-3}. Ion-exchange capacity of cation/anion-exchange resin (CR and AR) is 500 mol m^{-3}. Average diameter of resins is set as 0.5 mm. Volume fraction of CR and AR in MixR bed is set as 0.3. Void fraction of all the resin beds is set as 0.4 [24].

2.2. Ionic transport model

The ionic transport model of CC and membrane is the same as that in our previous study [12,16]. In DC of LayeredEDI, there exist three resin beds: CR bed, AR bed, and MixR bed. The mass conservation of species i at steady state is

$$\nabla \cdot \left(N_1^{\mathrm{DC}}\right) = -\varepsilon_\beta \nabla \cdot (U c_1) \tag{1}$$

$$\nabla \cdot \left(N_2^{\mathrm{DC}}\right) = -\varepsilon_\beta \nabla \cdot (U c_2) \tag{2}$$

$$\nabla \cdot \left(N_3^{\mathrm{DC}}\right) = -\varepsilon_\beta \nabla \cdot (U c_3) + \varepsilon_\beta K_w k_{-1}\left(1 - \frac{c_3 c_4}{K_w}\right) \tag{3}$$

$$\nabla \cdot \left(N_4^{\mathrm{DC}}\right) = -\varepsilon_\beta \nabla \cdot (U c_4) + \varepsilon_\beta K_w k_{-1}\left(1 - \frac{c_3 c_4}{K_w}\right) \tag{4}$$

where N_i^{DC} is the electrodiffusion flux of species i in DC; U is the velocity vector of flow. The electrodiffusion flux depends on the properties of the porous structure of resin bed; ε_β is the void fraction.

In CR bed,

$$N_1^{\mathrm{DC}} = -\left(\varepsilon_\beta \frac{D_{1,\mathrm{eff}} c_1}{RT} + \varepsilon_{\alpha C} \frac{D_{1,\mathrm{eff}}^{\alpha C} \frac{c_{\mathrm{CR}} c_1}{\alpha_1^3 c_3 + c_1}}{RT}\right)(RT \nabla \ln c_1 + z_1 F \nabla \varphi) - \varepsilon_\beta (D' - D_{1,\mathrm{eff}}) \nabla c_1 \tag{5}$$

$$N_2^{\mathrm{DC}} = -\varepsilon_\beta \frac{D_{2,\mathrm{eff}} c_2}{RT}(RT \nabla \ln c_2 + z_2 F \nabla \varphi) - \varepsilon_\beta (D' - D_{2,\mathrm{eff}}) \nabla c_2 \tag{6}$$

$$N_3^{\mathrm{DC}} = -\left(\varepsilon_\beta \frac{D_{3,\mathrm{eff}} c_3}{RT} + \varepsilon_{\alpha C} \frac{D_{3,\mathrm{eff}}^{\alpha C} \frac{c_{\mathrm{CR}} \alpha_1^3 c_3}{\alpha_1^3 c_3 + c_1}}{RT}\right)(RT \nabla \ln c_3 + z_3 F \nabla \varphi) - \varepsilon_\beta (D' - D_{3,\mathrm{eff}}) \nabla c_3 \tag{7}$$

Table 1
Values of the EDI cell parameters used for modeling

Parameter	Value	Ref.
Diffusion coefficient of Na^+, D_1	1.333×10^{-9} m^2 s^{-1}	[18]
Diffusion coefficient of Cl^-, D_2	2.033×10^{-9} m^2 s^{-1}	[18]
Diffusion coefficient of H^+, D_3	9.308×10^{-9} m^2 s^{-1}	[18]
Diffusion coefficient of OH^-, D_4	5.280×10^{-9} m^2 s^{-1}	[18]
Reference diffusion coefficient, D_0	1.0×10^{-9} $m^2 s^{-1}$	[18]
Diffusion coefficient of Na^+ in CM, D_1^{CM}	3.52×10^{-11} m^2 s^{-1}	[19]
Diffusion coefficient of H^+ in CM, D_3^{CM}	3.70×10^{-10} m^2 s^{-1}	[19]
Diffusion coefficient of Cl^- in AM, D_2^{AM}	3.91×10^{-11} m^2 s^{-1}	[19]
Diffusion coefficient of OH^- in AM, D_4^{AM}	5.28×10^{-11} m^2 s^{-1}	[19]
Separation factor between cation-exchange resin and solution phase, α_1^3	1	
Separation factor between anion-exchange resin and solution phase, α_2^4	1	
Ion-product constant of free water, K_w	1×10^{-8}	
Reverse direction reaction rate constant of water dissociation, k_{-1}	1.5×10^{-8}	
Reaction rate constant of deprotonation process, k_{-3}	1.5×10^{-7} m^3 mol^{-1} s^{-1}	[20,21]
Length of the cell, L	0.4 m	
Thickness of cation-exchange and anion-exchange membrane	0.4 mm	
Thickness of DC, d_{DC}	4 mm	
Thickness of CC, d_{CC}	4 mm	
Ion-exchange capacity of cation-exchange resin, c_{CR}	500 mol m^{-3}	
Ion-exchange capacity of cation-exchange resin, c_{AR}	500 mol m^{-3}	
Ion-exchange capacity of CM and AM, c_0^{CM}, c_0^{AM}	1,000 mol m^{-3}	
Average diameter of resins, d_p	0.5 mm	
Electrochemical transfer coefficient, ξ	0.5	[22,23]
Thickness of water dissociation layer on CM, λ_{CM}	10 nm	[22,23]
Thickness of water dissociation layer on AM, λ_{AM}	10 nm	[22,23]
Dilute compartment		
Salt concentration of feed water, c_0^{DC}	0.1 mol m^{-3}	
H^+ and OH^- concentrations of feed water, c_{HOH}	1.0×10^{-4} mol m^{-3}	
Inlet velocity, v_0^{DC}	0.05 m s^{-1}	
Volume fraction of cation-exchange resin, $v_{\alpha C}$	0.3	[24]
Volume fraction of anion-exchange resin, $\varepsilon_{\alpha A}$	0.3	[24]
Void fraction, ε_β	0.4	[24]
Concentrate compartment		
Salt concentration of feed water, c_0^{CC}	1 mol m^{-3}	
Inlet velocity, v_0^{CC}	0.05 m s^{-1}	

$$N_4^{DC} = -\varepsilon_\beta \frac{D_{4,eff} c_4}{RT}(RT\nabla \ln c_4 + z_4 F\nabla\varphi) - \varepsilon_\beta (D' - D_{4,eff})\nabla c_4 \quad (8)$$

In AR bed,

$$N_1^{DC} = -\varepsilon_\beta \left(\frac{D_{1,eff} c_1}{RT}\right)(RT\nabla \ln c_1 + z_1 F\nabla\varphi) - \varepsilon_\beta (D' - D_{1,eff})\nabla c_1 \quad (9)$$

$$N_2^{DC} = -\left(\varepsilon_\beta \frac{D_{2,eff} c_2}{RT} + \varepsilon_{\alpha A} \frac{D_{2,eff}^{\alpha A} \frac{c_{AR} c_1}{\alpha_1^3 c_3 + c_1}}{RT}\right)(RT\nabla \ln c_2 + z_2 F\nabla\varphi) - \varepsilon_\beta (D' - D_{2,eff})\nabla c_2 \quad (10)$$

$$N_3^{DC} = -\left(\varepsilon_\beta \frac{D_{3,eff} c_3}{RT}\right)(RT\nabla \ln c_3 + z_3 F\nabla\varphi) - \varepsilon_\beta (D' - D_{3,eff})\nabla c_3 \quad (11)$$

$$N_4^{DC} = -\left(\varepsilon_\beta \frac{D_{4,eff} c_4}{RT} + \varepsilon_{\alpha A} \frac{D_{4,eff}^{\alpha A} \frac{c_{AR} \alpha_2^4 c_4}{\alpha_2^4 c_4 + c_2}}{RT}\right)(RT \nabla \ln c_4 + z_4 F \nabla \varphi) - \varepsilon_\beta (D' - D_{4,eff}) \nabla c_4 \quad (12)$$

In MixR bed,

$$N_1^{DC} = -\left(\varepsilon_\beta \frac{D_{1,eff} c_1}{RT} + \varepsilon_{\alpha C} \frac{D_{1,eff}^{\alpha C} \frac{c_{CR} c_1}{\alpha_1^3 c_3 + c_1}}{RT}\right)(RT \nabla \ln c_1 + z_1 F \nabla \varphi) - \varepsilon_\beta (D' - D_{1,eff}) \nabla c_1 \quad (13)$$

$$N_2^{DC} = -\left(\varepsilon_\beta \frac{D_{2,eff} c_2}{RT} + \varepsilon_{\alpha A} \frac{D_{2,eff}^{\alpha A} \frac{c_{AR} c_1}{\alpha_1^3 c_3 + c_1}}{RT}\right)(RT \nabla \ln c_2 + z_2 F \nabla \varphi) - \varepsilon_\beta (D' - D_{2,eff}) \nabla c_2 \quad (14)$$

$$N_3^{DC} = -\left(\varepsilon_\beta \frac{D_{3,eff} c_3}{RT} + \varepsilon_{\alpha C} \frac{D_{3,eff}^{\alpha C} \frac{c_{CR} \alpha_1^3 c_3}{\alpha_1^3 c_3 + c_1}}{RT}\right)(RT \nabla \ln c_3 + z_3 F \nabla \varphi) - \varepsilon_\beta (D' - D_{3,eff}) \nabla c_3 \quad (15)$$

$$N_4^{DC} = -\left(\varepsilon_\beta \frac{D_{4,eff} c_4}{RT} + \varepsilon_{\alpha A} \frac{D_{4,eff}^{\alpha A} \frac{c_{AR} \alpha_2^4 c_4}{\alpha_2^4 c_4 + c_2}}{RT}\right)(RT \nabla \ln c_4 + z_4 F \nabla \varphi) - \varepsilon_\beta (D' - D_{4,eff}) \nabla c_4 \quad (16)$$

where c_i and φ are the concentration and potential in solution phase, respectively; $D_{i,eff}$, $D_{i,eff}^{\alpha C}$ and $D_{i,eff}^{\alpha A}$ are the effective diffusion coefficients of species i in the corresponding phase; D' is the hydrodynamic dispersion tensor, which is composed of the longitudinal (y-direction) and the transversal (x-direction) dispersion coefficients: D'_L and D'_T. The definitions of these parameters could be found in our previous study [12,16]; $\varepsilon_{\alpha C}$ and $\varepsilon_{\alpha A}$ are the volume fraction of cation-exchange resin phase and anion-exchange resin phase, respectively.

The final equation for electric potential can be deduced from the conservation of electric charge, which states that

$$\nabla \cdot J^{DC} = 0 \quad (17)$$

where the local current density J^{DC} is given by the Faraday's law,

$$J^{DC} = F \sum_{i=1}^{4} z_i \cdot N_i^{DC} \quad (18)$$

where N_i^{DC} is electrodiffusion flux of species i in DC, which is composed of the flux of diffusion and migration. The electro-neutrality condition dominates over the whole domain and states

$$\sum_{i=1}^{4} z_i \cdot c_i = 0 \quad (19)$$

With this restriction, c_4 could be considered as a function of c_1, c_2, and c_3.

Thus, the mass conservation equations of species 1–3 (Eqs. (1)–(3)) and the equation of electric charge (Eq. (19)) compose the governing equations for solving four unknowns: c_1, c_2, c_3, and φ in DC.

2.3. Boundary conditions

2.3.1. External boundary conditions

Uniform concentration is assumed at the inlet of each compartment. The salt ions concentration at the inlet of DC and CC is set as c_0^{DC} and c_0^{CC}, respectively. The feed water of DC and CC is neutral. A potential difference φ_0 is given over the cell. The external boundary conditions of LayeredEDI are the same as that of MixREDI and CREDI [12,16].

2.3.2. Internal boundary conditions

Donnan equilibrium prevails at the internal boundaries. The concentration of species at the membrane–solution interface fulfills the traditional Donnan relations [12,16]. The electric potential jump at the internal boundaries is obtained by the Donnan potential. This gives restrictions for the potential in each compartment. The continuity of ionic flux and the current must be maintained for the internal boundaries. The

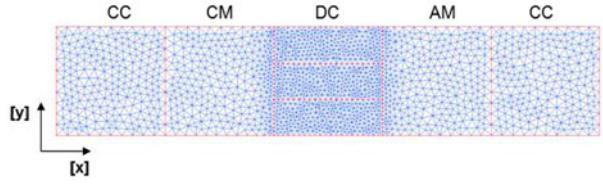

Fig. 3. Mesh configuration of layered bed EDI cell.

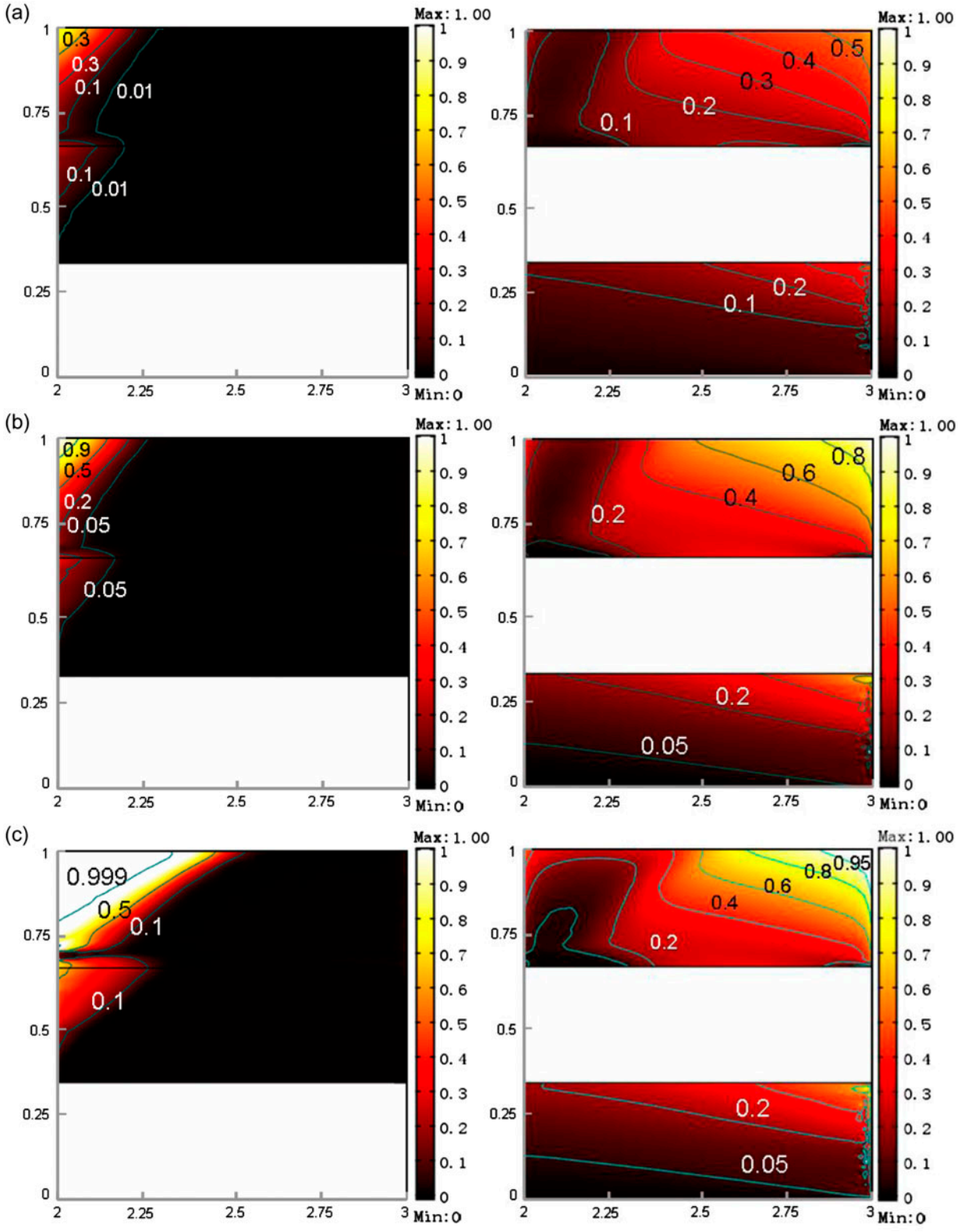

Fig. 4. Transformation ratio of anion-exchange resin (left) and CREDI (right) in DC of LayeredEDI at various average current densities: (a) $J = 24.85$ A m^{-2}; (b) $J = 37.95$ A m^{-2}; (c) $J = 54.58$ A m^{-2}.

continuity of the flux at different internal boundaries is presented as:

$$N_1^{CC}|_{x=1^-} = N_1^{CM}|_{x=1^+};\ N_2^{CC}|_{x=1^-} = 0;\ N_3^{CC}|_{x=1^-} = -N_1^{CC}|_{x=1^-} + \frac{J^{CC}|_{x=1^-}}{F};\ J^{CC}|_{x=1^-} = J^{CM}|_{x=1^+} \quad (20)$$

$$N_1^{CM}|_{x=2^-} = N_1^*|_{x=2^+};\ 0 = N_2^*|_{x=2^+};\ N_3^{CM}|_{x=2^-} + \frac{i_w^{CM}\cdot\lambda_{CM}}{F} = N_3^*|_{x=2^+};\ J^{CM}|_{x=2^-} = J^{DC}|_{x=2^+} \quad (21)$$

$$N_1^{DC}|_{x=3^-} = 0;\ N_2^{DC}|_{x=3^-} = N_2^{AM}|_{x=3^+};\ N_3^{DC}|_{x=3^-} + \frac{i_w^{AM}\cdot\lambda_{AM}}{F} = 0;\ J^{DC}|_{x=3^-} = J^{AM}|_{x=3^+} \quad (22)$$

$$0 = N_1^{CC}|_{x=4^+};\ N_2^{AM}|_{x=4^-} = N_2^{CC}|_{x=4^+};\ 0 = N_3^{CC}|_{x=4^+};\ J^{AM}|_{x=4^-} = J^{CC}|_{x=4^+} \quad (23)$$

where λ_{CM} and λ_{AM} are the thickness of the water dissociation layers at the surface of CM and AM,

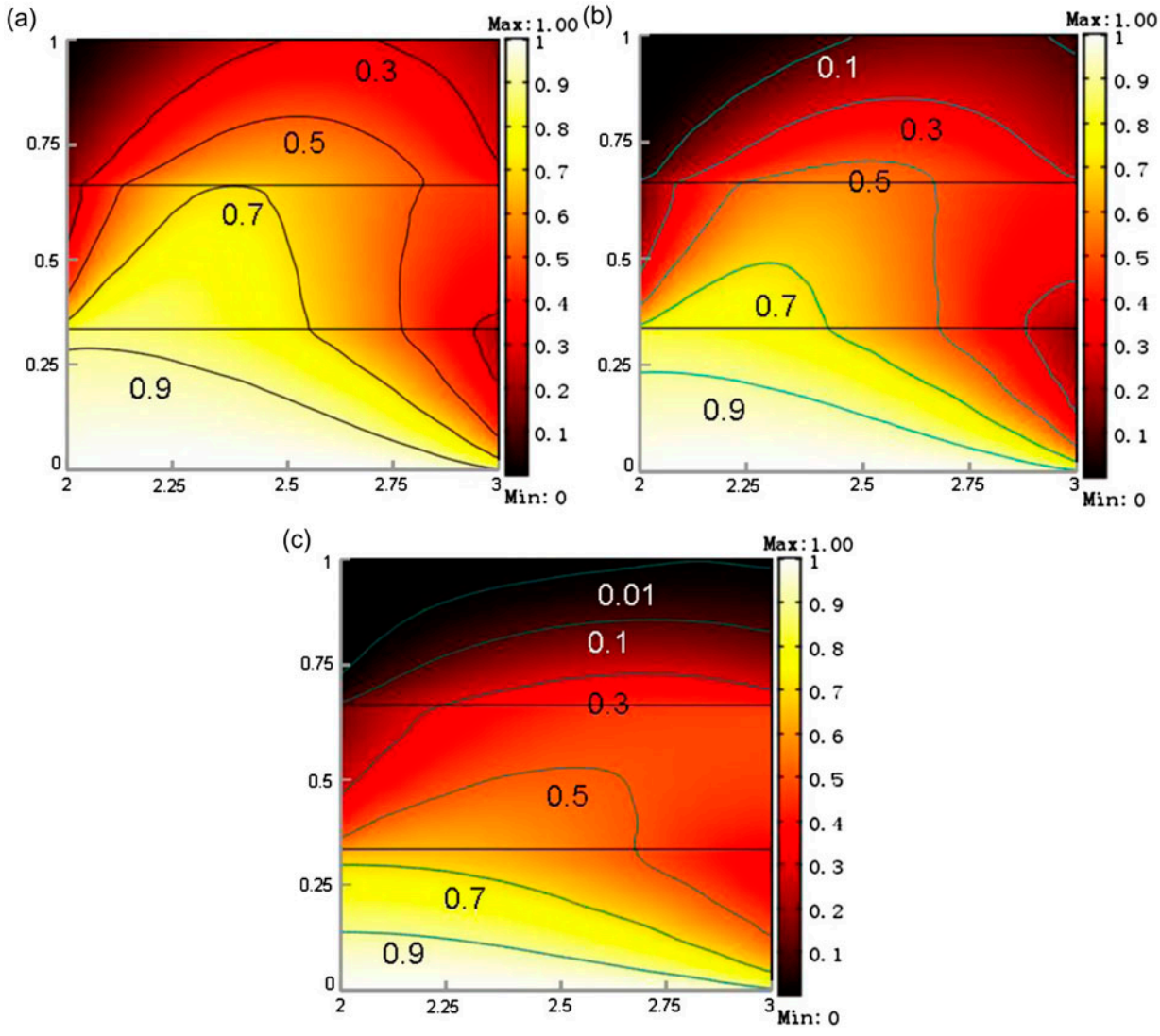

Fig. 5. Concentration distribution of salt cation in solution phase of DC in LayeredEDI at various average current densities: (a) J = 24.85 A m^{-2}; (b) J = 37.95 A m^{-2}; (c) J = 54.58 A m^{-2}.

respectively. They are assumed to be equal to the thickness of σ region; i_w^{CM} and i_w^{AM} are the water dissociation current at CM–DC and AM–DC interface, respectively.

The water dissociation intensity depends on the concentration polarization intensity and the catalytic group concentration, and water dissociation current at each layer of DC is specified [12,16].

CM–CR bed interface:

$$i_w^{CM-CR} = FK_w k_{-1}\left(\frac{c_{CM}}{c_1+c_3}\right)^{\xi}\left(1-\frac{c_3c_4}{K_w}\right) \quad (24)$$

AM–CR bed interface:

$$i_w^{AM-CR} = FK_w k_{-3} c_{BH^+}^{AM-CR} 10^{pK_b}\left(\frac{c_{AM}}{c_2+c_4}\right)^{\xi}\left(1-\frac{c_3c_4}{K_w}\right) \quad (25)$$

CM–AR bed interface:

$$i_w^{CM-AR} = FK_w k_{-3} c_{BH^+}^{CM-AR} 10^{pK_b}\left(\frac{c_{AM}}{c_2+c_4}\right)^{\xi}\left(1-\frac{c_3c_4}{K_w}\right) \quad (26)$$

AM–AR bed interface:

$$i_w^{AM-AR} = FK_w k_{-3} c_{BH^+}^{AM-AR} 10^{pK_b}\left(\frac{c_{AM}}{c_2+c_4}\right)^{\xi}\left(1-\frac{c_3c_4}{K_w}\right) \quad (27)$$

CM–MixR bed interface:

$$i_w^{CM-MixR} = FK_w k_{-3} c_{BH^+}^{CM-MixR} 10^{pK_b}\left(\frac{c_{CM}}{c_1+c_3}\right)^{\xi}\left(1-\frac{c_3c_4}{K_w}\right) \quad (28)$$

AM–MixR bed interface:

$$i_w^{AM-MixR} = FK_w k_{-3} c_{BH^+}^{Am-MixR} 10^{pK_b}\left(\frac{c_{AM}}{c_2+c_4}\right)^{\xi}\left(1-\frac{c_3c_4}{K_w}\right) \quad (29)$$

where $c_{BH^+}^{Am-CR}$, $c_{BH^+}^{CM-AR}$, $c_{BH^+}^{AM-AR}$, $c_{BH^+}^{CM-MixR}$ and $c_{BH^+}^{AM-MixR}$ are the concentration of catalytic group (tertiary ammonium groups) at AM–CR bed, CM–AR bed, AM–AR bed, CM–MixR bed, and AM–MixR bed interface, respectively, and are equal to c_{AM}, $0.18c_{AR}$, c_{AM}, $0.09c_{AR}$, and c_{AM} [25].

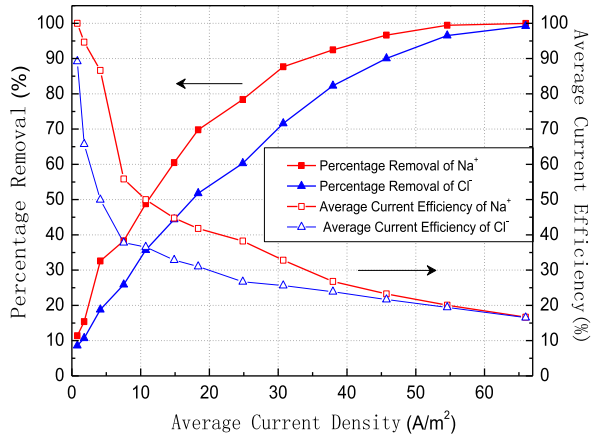

Fig. 6. Removal efficiency and average current efficiency of LayeredEDI as a function of average current density.

2.4. Numerical solution

The finite element commercial software, COMSOL Multiphysics, is used to solve the partial differential equations. The mesh configuration is illustrated in Fig. 3. The method converges when the weighted absolute residual norm is less than 10^{-6}. The stationary segregated nonlinear solver of COMSOL software was chosen as the solver.

3. Results and discussion

The DC of LayeredEDI is composed of three different resin beds. From the inlet to the outlet, there are cation-exchange resin bed, anion-exchange resin bed, and MixR bed. At the inlet area is the cation-exchange resin bed (CR bed). The concentration polarization is not intense at the inlet. Thus, the water dissociation at AM–CR bed interface is not intense. Therefore, the CREDI is still in salt form (Fig. 4). In our previous work [16], it was concluded that, when the concentration of salt ions in solution phase is high, the salt-form resins could enhance the electro-migration flux of salt ions. The concentration of salt ions at the inlet area is much high. Thus, the CR bed becomes a high conductivity channel for salt cations. A large amount of salt cations are removed through this layer. The concentration distribution of salt cation is illustrated in Fig. 5. Through CR bed, half of the salt cation is reduced.

At the outlet area is the MixR bed. The concentration polarization of salt ions at membrane surface is intense. Water dissociation at CM and AM surface is

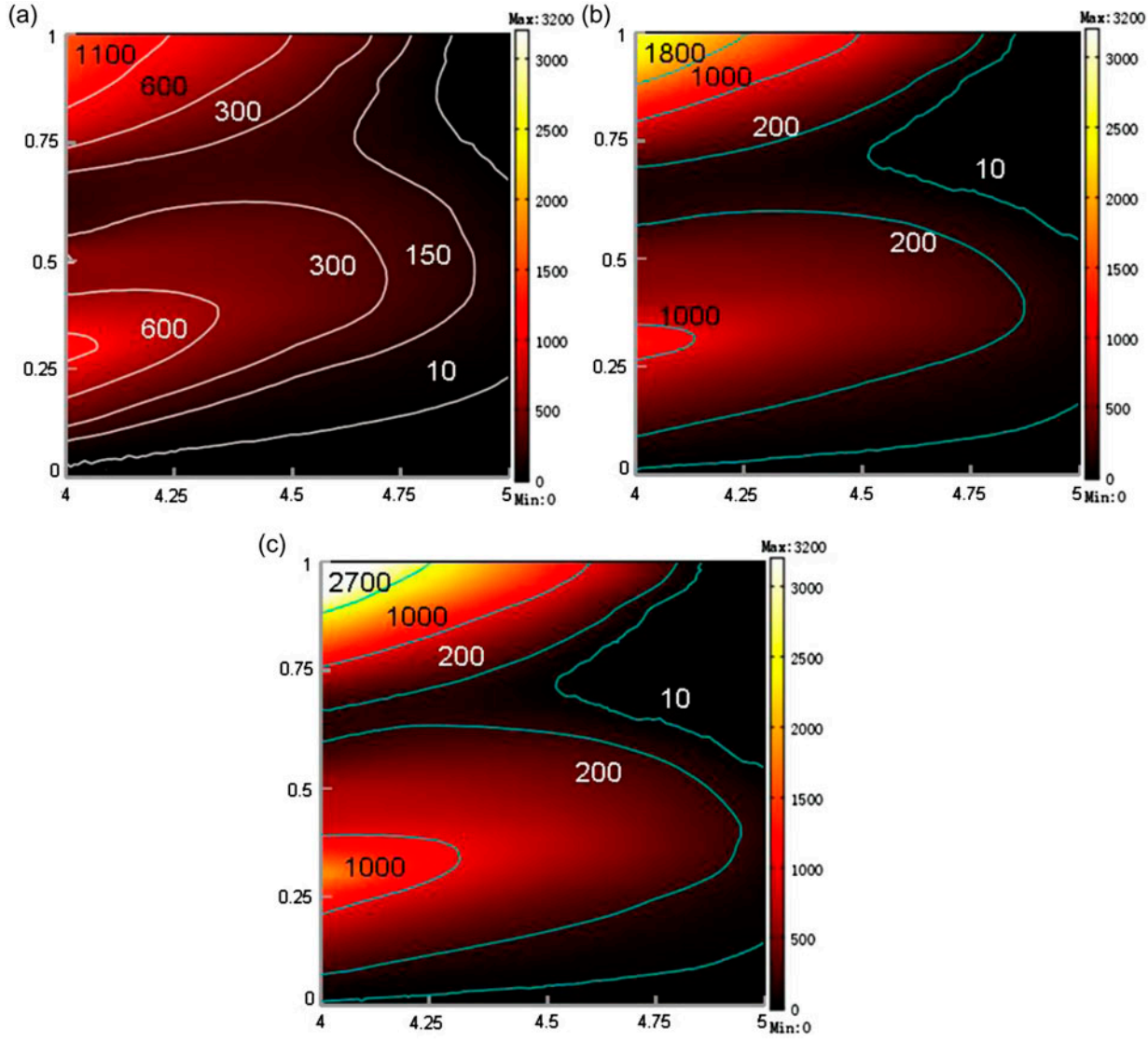

Fig. 7. Concentration distribution of OH^- in CC-2 of LayeredEDI at various average current densities: (a) $J = 24.85$ A m^{-2}; (b) $J = 37.95$ A m^{-2}; (c) $J = 54.58$ A m^{-2}.

thus intense and makes the cation and anion-exchange resins regenerated (see Fig. 4). In our previous investigation [14], it was concluded that the regenerated resin could enhance the electro-migration flux of the salt ions in the interstitial solution phase where the concentration of salt ions is much low. Therefore, the concentration of salt ions is much low. This makes the salt cation and anion depleted, and the concentration of salt ions is much low (Fig. 5). The most important factor for this layer is that the water dissociation at AM–DC interface of MixR bed is much lower than that of CR bed. This will reduce the precipitations at AM–CC interface. It will be discussed in the following part.

The salt anion also needs to be separated. Thus, between CR bed and MixR bed, an anion-exchange resin bed (AR bed) is fixed. This layer produces a high-conductivity channel for salt anions. In this layer, the concentration of salt anions is high (Fig. 5) and the anion-exchange resin is also in salt form (Fig. 4).

In order to compare LayeredEDI with CREDI, the removal percentage and current efficiency are investigated (Fig. 6). In LayeredEDI, at $J = 56$ A m^{-2}

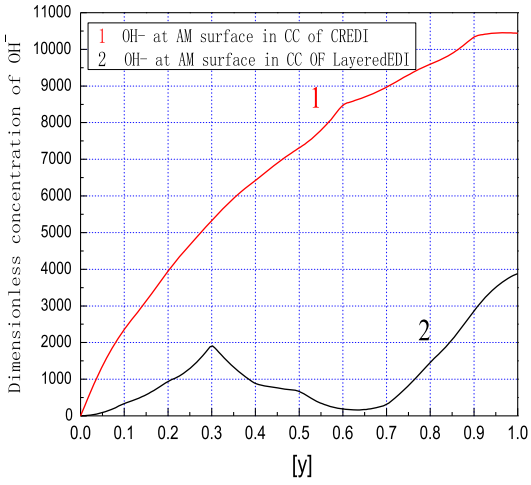

Fig. 8. At the same salt cation removal percentage (99.5%), the distribution of OH^- concentration at AM–CC interface in LayeredEDI and CREDI.

the percentage of salt cation achieves at 95.5% and the current efficiency is about 22%. However, in CREDI, at the same removal percentage, the average current density is much larger and is about 90 A m^{-2}; the current efficiency of salt cation is 14%. The energy consumption of LayeredEDI is lower than that of CREDI. This could be explained by the water dissociation and concentration polarization difference between LayeredEDI and CREDI. At the outlet of LayeredEDI and CREDI is the MixR bed and CR bed, respectively. Since at the same cell voltage the concentration polarization of EDI with MixR bed is less intense than that of EDI with CR bed, the flux of salt cation in MixR bed is thus much larger than that of CR bed [12]. Also at the same cell voltage, the excessive water dissociation produced in MixR bed is lower than that of CR bed, and the result is that the current efficiency of MixR bed is larger than that of CR bed [12].

In CREDI, since H^+ dominates the solution phase of DC, there is no hydroxide precipitation in DC. However, in CC, the OH^- originated from water dissociation at AM–DC interface combines with heavy metal ions. Thus, the precipitation in CC is intense [16]. The OH^- concentration profile in CC of LayeredEDI is illustrated in Fig. 7. Since there is water dissociation catalyst at AM surface, the water dissociation at AM–DC interface is much intense. The water dissociation products OH^- migrates through AM to CC. Due to the fact that the transport number difference between AR bed and AM is much low, the concentration polarization at AR bed is less intense [16]. The result is that the water dissociation at DC–AM interface of the AR bed is less intense. Therefore, the OH^- concentration at the corresponding area in CC is also low. Thus in Fig. 7, there exists two OH^- concentration peaks at AM–CC interface (i.e. the risk of hydroxide precipitation is much high in those two areas).

At the same percentage removal of salt cation, the average current density of LayeredEDI is lower than that of CREDI. The current efficiency of LayeredEDI is larger than that of CREDI. Thus, the water dissociation current density of LayeredEDI is lower than that of CREDI. Therefore, the concentration of OH^- at CC–AM interface of LayeredEDI is much lower than that of CREDI. At the same salt cation removal percentage (99.5%), the comparison of OH^- concentration at the interface of CC–AM in LayeredEDI and CREDI is illustrated in Fig. 8. The LayeredEDI reduces hydroxide precipitation to a much lower level. In addition, it is necessary to mention that the high-risk precipitation area at AM surface in CC is at the same horizontal level as the interface of CR bed and AR bed.

The behavior of H^+ transportation in DC is investigated. Concentration distribution of OH^- (left) and H^+ (right) in solution phase of DC in LayeredEDI is illustrated in Fig. 9. Water dissociation at CM–DC interface produces OH^-. It will bring precipitation at CM–DC interface. Thus, the high-precipitation area is found at CM–DC interface where water dissociation is intense. At the inlet, the concentration polarization in CR bed layer is not intense. The water dissociation at this layer is negligible. In AR bed layer, water dissociation catalyst on anion-exchange resin in AR bed makes water dissociation at CM–DC surface much intense. The result is that the concentration of OH^- is large in this layer. However, even at $J = 54.58$ A m^{-2}, the maximum OH^- concentration is about 8×10^{-6} mol/L. It is because that the OH^- originated from CM–AR bed interface combines with the H^+ of the convection fluid from CR bed and the H^+ originated from water dissociation at AM–AR bed interface. OH^- concentration at this level is much low. Therefore, the precipitation is negligible. At the outlet area, H^+ originated from AM–MixR bed interface combines with the OH^- from CM–MixR bed interface. OH^- concentration is much low. The reason why the high-concentration area is in AR bed is that anion-exchange resin has water dissociation catalyst.

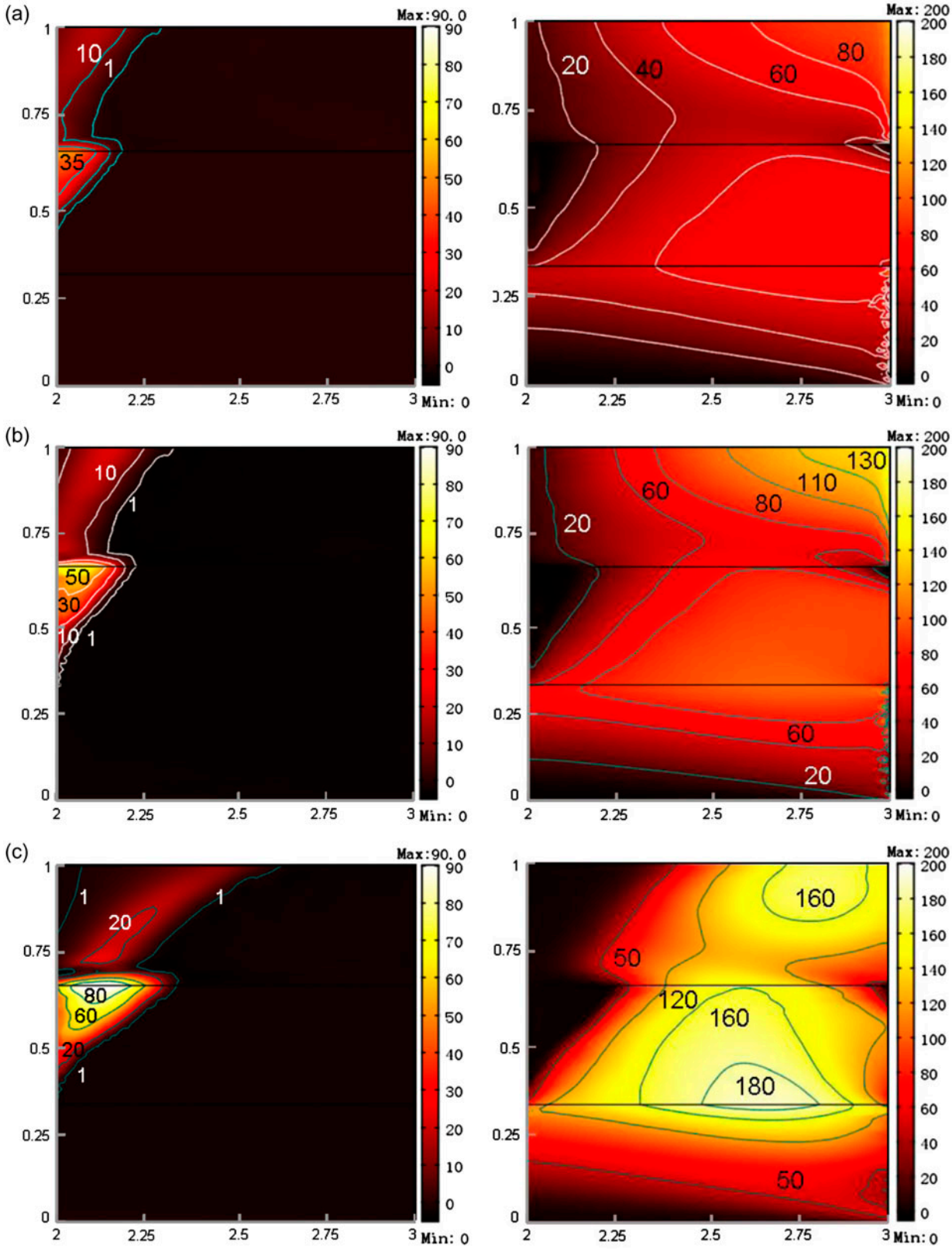

Fig. 9. Concentration distribution of OH^- (left) and H^+ (right) in solution phase of DC in LayeredEDI: (a) J = 24.85 A m^{-2}; (b) J = 37.95 A m^{-2}; (c) J = 54.58 A m^{-2}.

4. Conclusions

A numerical steady state model was established to describe the process of EDI with DC fixed with layered resin bed for deeply separating salt ions. At the inlet area of DC is CR bed. The CREDI is still in salt form, and it produces a high-conductivity channel for salt cations of high concentration. At the outlet is MixR bed. In this layer, the concentration of salt cation and anion are both low. The regenerated mixed resin could also produce a high-conductivity channel for salt cation and anion. The appropriate water dissociation at this layer is produced. Thus at the same percentage removal, the average current density of LayeredEDI is much lower than that of CREDI. The current efficiency of LayeredEDI is much larger than that of CREDI. In CC, the OH^- concentration at AM–CC interface of LayeredEDI is much lower than that of CREDI. The risk of hydroxide precipitation is reduced. However, there exist two OH^- concentration peaks at AM–CC interface and the hydroxide precipitation is usually centered on those two areas. The simulation results show that the OH^- concentration in DC is negligible. The highest concentration area is at CM–CR bed interface.

Acknowledgments

This study was supported by the National Natural Science Foundation of China (NSFC No. 51208233) and the Natural Science Foundation of Jiangsu Province, China (No. BK2012079). This work was supported by the Priority Academic Program Development of Jiangsu Higher Education Institutions (PAPD).

Nomenclature

MixREDI — EDI with dilute compartment fixed with mixed cation-exchange and anion-exchange resins
CREDI — EDI with dilute compartment fixed with cation-exchange resins
LayeredEDI — EDI with dilute compartment fixed with layered resin beds
MixR bed — mixed cation-exchange and anion-exchange resin bed
CR bed — cation-exchange resin bed
AR bed — anion-exchange resin bed
CC — concentrated compartment
CC-1 — left concentrated compartment
CC-2 — right concentrated compartment
DC — dilute compartment
CM — cation-exchange membrane
AM — anion-exchange membrane
c_i — concentration of species i in interstitial solution phase of DC (mol m^{-3})
c_{CR} — ion-exchange capacity of cation-exchange resin (mol m^{-3})
c_{AR} — ion-exchange capacity of cation-exchange resin (mol m^{-3})
c_0^{CC} — salt concentration of feed water of CC (mol m^{-3})
c_0^{DC} — salt concentration of feed water of DC (mol m^{-3})
c_{HOH} — H^+ and OH^- concentration of feed water in DC and CC (mol m^{-3})
c_{CM} — ion-exchange capacity of CM (mol m^{-3})
c_{AM} — ion-exchange capacity of AM (mol m^{-3})
$c_{BH^+}^{AM-CR}$ — concentration of catalytic group at AM–CR bed interface
$c_{BH^+}^{AM-AR}$ — concentration of catalytic group at AM–AR bed interface
$c_{BH^+}^{AM-MixR}$ — concentration of catalytic group at AM–MixR bed interface
$c_{BH^+}^{CM-AR}$ — concentration of catalytic group at CM–AR bed interface
$c_{BH^+}^{CM-MixR}$ — concentration of catalytic group at CM–MixR bed interface
D_i — diffusion coefficient of species i (mol m^{-2} s^{-1})
D_0 — reference diffusion coefficient (mol m^{-2} s^{-1})
$D_{i,eff}$ — effective diffusion coefficient of i in interstitial solution phase (mol m^{-2} s^{-1})
$D_{i,eff}^{\alpha C}$ — effective diffusion coefficient of species i in cation-exchange resin phase (mol m^{-2} s^{-1})
$D_{i,eff}^{\alpha A}$ — effective diffusion coefficient of species i in anion-exchange resin phase (mol m^{-2} s^{-1})
D' — hydrodynamic dispersion tensor (mol m^{-2} s^{-1})
D_L' — longitudinal dispersion coefficients (mol m^{-2} s^{-1})
D_T' — transverse dispersion coefficients (mol m^{-2} s^{-1})
F — Faraday's constant
i_w^{CM-CR} — current density of water dissociation at CM and CR bed interface (A m^{-2})
i_w^{CM-AR} — current density of water dissociation at CM and AR bed interface (A m^{-2})
$i_w^{CM-MixR}$ — current density of water dissociation at CM and MixR bed interface (A m^{-2})
i_w^{AM-CR} — current density of water dissociation at AM and CR bed interface (A m^{-2})
i_w^{AM-AR} — current density of water dissociation at AM and AR bed interface (A m^{-2})
$i_w^{AM-MixR}$ — current density of water dissociation at AM and MixR bed interface (A m^{-2})
J — average current density (A m^{-2})
J^{DC} — local current density in DC (A m^{-2})
K_w — ion-product constant of water
k_1 — forward reaction rate constant of water dissociation

k_{-1} — backward reaction rate constant of water dissociation
k_2 — forward reaction rate constant of the protonation
k_{-2} — backward reaction rate constant of the protonation
k_3 — forward reaction rate constant of the deprotonation
k_{-3} — forward reaction rate constant of the deprotonation
K_b — equilibrium constant of the protonation
K — the permeability of particle porous bed
N_i^{DC} — electrodiffusion flux of species i in DC (mol m^{-2} s^{-1})
N_i^{CC} — electrodiffusion flux of species i in CC (mol m^{-2} s^{-1})
N_i^{CM} — electrodiffusion flux of species i in CM (mol m^{-2} s^{-1})
N_i^{AM} — electrodiffusion flux of species i in AM (mol m^{-2} s^{-1})
R_i — generation rate or annihilation rate of H^+ or OH^- (mol m^{-3} s^{-1})
R_w — water dissociation reaction rate (mol m^{-3} s^{-1})
U — velocity vector of flow
z_i — charge number of species i

Greek symbols

αA — cation-exchange resin phase
αC — anion-exchange resin phase
β — interstitial solution phase
ε_β — void fraction
$\varepsilon_{\alpha C}$ — volume fraction of cation-exchange resin phase
$\varepsilon_{\alpha A}$ — volume fraction of anion-exchange resin phase
λ_{CM} — thickness of water dissociation layer at the surface of CM (m)
λ_{AM} — thickness of water dissociation layer at the surface of AM (m)
φ — electric potential in interstitial solution phase of dilute compartment (V)

Subscripts

1 — Na^+
2 — Cl^-
3 — H^+
4 — OH^-
AM — anion-exchange membrane
CM — cation-exchange membrane
AR — anion-exchange resin
CR — cation-exchange resin

References

[1] L. Alvarado, A.C. Chen, Electrodeionization: Principles, strategies and applications, Electrochim. Acta 132 (2014) 583–597.
[2] I.G. Wenten, Khoiruddin, F. Arfianto, Zudiharto, Bench scale electrodeionization for high pressure boiler feed water, Desalination 314 (2013) 109–114.
[3] Ö. Arar, Ü. Yüksel, N. Kabay, M. Yüksel, Demineralization of geothermal water reverse osmosis (RO) permeate by electrodeionization (EDI) with mixed bed configuration, Desalination 342 (2014) 23–28.
[4] Y.S. Dzyazko, L.N. Ponomaryova, L.M. Rozhdestvenskaya, S.L. Vasilyuk, V.N. Belyakov, Electrodeionization of low-concentrated multicomponent Ni^{2+}-containing solutions using organic–inorganic ion-exchanger, Desalination 342 (2014) 43–51.
[5] W. Su, R. Pan, Y. Xiao, X.M. Chen, Membrane-free electrodeionization for high purity water production, Desalination 329 (2013) 86–92.
[6] W.Q. Su, T.J. Li, X.P. Jiang, X.M. Chen, Membrane-free electrodeionization without electrode polarity reversal for high purity water production, Desalination 345 (2014) 50–55.
[7] K.H. Yeon, J.H. Song, S.H. Moon, A study on stack configuration of continuous electrodeionization for removal of heavy metal ions from the primary coolant of a nuclear power plant, Water Res. 38 (2004) 1911–1921.
[8] Y.S. Dzyazko, Purification of a diluted solution containing nickel using electrodeionization, Desalination 198 (2006) 47–55.
[9] L.M. Rozhdestvenska, Y.S. Dzyazko, V.N. Belyakov, Electrodeionization of a Ni^{2+} solution using highly hydrated zirconium hydrophosphate, Desalination 198 (2006) 247–255.
[10] X. Feng, Z.C. Wu, X.F. Chen, Removal of metal ions from electroplating effluent by EDI process and recycle of purified water, Sep. Purif. Technol. 57 (2007) 257–263.
[11] M.J. Semmens, C.D. Dillon, C. Riley, An evaluation of continuous electrodeionization as an in-line process for plating rinsewater recovery, Environ. Prog. 20 (2001) 251–260.
[12] J. Lu, Y.X. Wang, Y.Y. Lu, G.L. Wang, L. Kong, J. Zhu, Numerical simulation of the electrodeionization (EDI) process for producing ultrapure water, Electrochim. Acta 55 (2010) 7188–7198.
[13] L. Fu, J.Y. Wang, Y.L. Su, Removal of low concentrations of hardness ions from aqueous solutions using electrodeionization process, Sep. Purif. Technol. 68 (2009) 390–396.
[14] K.H. Yeon, J.H. Seong, S. Rengaraj, S.H. Moon, Electrochemical characterization of ion-exchange resin beds and removal of cobalt by electrodeionization for high purity water production, Sep. Sci. Technol. 38 (2003) 443–462.
[15] J.W. Lee, K.H. Yeon, J.H. Song, S.H. Moon, Characterization of electroregeneration and determination of optimal current density in continuous electrodeionization, Desalination 207 (2007) 276–285.
[16] J. Lu, Y.X. Wang, J. Zhu, Numerical simulation of the electrodeionization (EDI) process accounting for water dissociation, Electrochim. Acta 55 (2010) 2673–2686.
[17] A. Mahmoud, L. Muhr, S. Vasiluk, A. Aleynikoff, F. Lapicque, Investigation of transport phenomena in a hybrid ion exchange-electrodialysis system for the removal of copper ions, J. Appl. Electrochem. 33 (2003) 875–884.

[18] R.H. Perry, Perry's Chemical Engineers' Handbook, seventh ed., McGraw-Hill Professional, New York, NY, 1999.
[19] C.O. Danielsson, A. Dahlkild, A. Velin, M. Behm, Nitrate removal by continuous electropermutation using ion-exchange textile I. Modeling, J. Electrochem. Soc. 153 (2006) 51–61.
[20] R. Simons, Water splitting in ion-exchange membranes, Electrochim. Acta 30 (1985) 275–282.
[21] R. Simons, Electric field effects on proton transfer between ionizable groups and water in ion exchange membranes, Electrochim. Acta 29 (1984) 151–158.
[22] H.D. Hurwitz, R. Dibiani, Investigation of electrical properties of bipolar membranes at steady state and with transient methods, Electrochim. Acta 47 (2001) 759–773.
[23] H.D. Hurwitz, R. Dibiani, Experimental and theoretical investigations of steady and transient states in systems of ion exchange bipolar membranes, J. Membr. Sci. 228 (2004) 17–43.
[24] J. Bear, Dynamics of Fluids in Porous Media, American Elsevier, New York, NY, 1972.
[25] J. Lu, A Study on Numerical Simulation of the Electrodeionization Process, Ph.D. thesis, Tianjin University, 2009.